https://doi.org/10.5194/egusphere-2026-3377
Preprint. Discussion started: 14 September 2026

Mimetic interpolation for finite-time Lyapunov exponent computation near irregular domain boundaries

Tamara Pletzer[1], Alexander Pletzer[2], Timothy C. Andrews[3], Dongqi Lin[4,5], and Marwan Katurji[1]

[1]School of Earth and Environment, University of Canterbury, Christchurch, New Zealand
[2]Research Education Advanced Network New Zealand (REANNZ), Wellington, New Zealand
[3]Department of Climate and Space Sciences and Engineering, University of Michigan, Ann Arbor, MI, USA
[4]The ARC Centre of Excellence for Climate Extremes, Monash University, Melbourne, Victoria, Australia
[5]School of Earth, Atmosphere and Environment, Monash University, Melbourne, Victoria, Australia

Correspondence: Tamara Pletzer (tamara.pletzer@canterbury.ac.nz)

Abstract. Finite-time Lyapunov exponents (FTLEs) are widely used to identify Lagrangian coherent structures (LCS) in geophysical flows. Applying FTLEs to numerical model output requires reconstructing continuous velocity fields from discrete model grids, thus the resulting flow structures are sensitive to the interpolation method. This issue is particularly important for models with staggered-grid discretisations and complex solid boundaries, such as buildings, terrain and coastlines, where velocity components are defined at different locations and no-through-flow conditions must be respected. Most existing FTLE workflows assume co-located velocity components and do not explicitly account for fluid-solid boundaries during interpolation. Interpolating staggered velocities to cell centres before trajectory integration can therefore violate boundary conditions, producing unphysical particle paths, including trajectories that enter solid regions. Here, we present a flux-conservative, mimetic vector interpolation scheme that removes the co-location assumption while ensuring no-through-flow conditions at fluid-solid interfaces. We demonstrate the method using large eddy simulations of a wildfire plume in urban terrain. Compared with conventional interpolation, the mimetic approach produces boundary-aware trajectories and reveals coherent-structure geometries shaped by urban topography that are otherwise obscured. These results show that interpolation is not merely a numerical preprocessing step, but can directly affect inferred LCS geometries and their physical interpretation in staggered-grid simulations with complex boundaries.

1 Motivation

Finite-time Lyapunov exponents (FTLEs) are increasingly being used in geophysical fluids as a mathematically rigorous method to define material transport boundaries in the velocity field. For example, they have been used to show marine food web activity converges along FTLE boundaries (Veatch et al., 2025), to track oil spill plumes and manage clean-ups (Spaulding, 2017), and to explain Saharan dust transport (Jarvis et al., 2024). FTLEs are a hyperbolic case of Lagrangian coherent structure (LCS) analysis, a frame indifferent method to mathematically delineate different coherent structure geometries (Haller, 2015). FTLEs show the regions of the greatest attractors and repellers in the flow (dependent on integration direction) and are analogous to stable and unstable manifolds in chaotic dynamical systems. Yet computing FTLEs and LCS from numerical model

https://doi.org/10.5194/egusphere-2026-3377
Preprint. Discussion started: 14 September 2026

output is non-trivial, because trajectory integration depends on how discrete velocity fields are reconstructed, and errors in this reconstruction can directly affect the inferred coherent structures.

The fundamental challenge in computing FTLEs from numerical model output is that the calculation often requires a co-located velocity vector, yet most geophysical models output velocity on a staggered grid. Geophysical models, including atmospheric and oceanic, often discretise the momentum equations on the Arakawa C-grid (Arakawa and Lamb, 1977), where each velocity component is defined at different cell faces rather than at a common set of grid points (e.g. Fig. 1). This staggering improves the accuracy of the discrete divergence and pressure gradient operators, but it means that no single grid location carries the full velocity vector. Working directly with the native staggered output is thus preferable on physical grounds, but requires an interpolation scheme that respects the staggered geometry and preserves the properties for which the staggered discretisation was designed.

A further complication arises from the treatment of solid boundaries within the computational domain. Many geophysical models employ Cartesian (non-terrain-following) grids, so complex terrain, buildings, and other solid obstacles intersect the computational grid arbitrarily. Grid points that lie below the terrain surface or within solid structures are not part of the fluid domain and carry no physical velocity. Different models handle this differently: some mask these points as NaN (Not a Number), some assign a zero, and others exclude them from the output entirely. Any interpolation stencil that spans the fluid-solid interface will draw on points that are undefined or physically meaningless, contaminating the interpolated velocity and potentially allowing particle trajectories to penetrate solid regions. Near the interface, the number of valid grid points available to the stencil is also reduced, forcing either a degradation in interpolation order or an explicit one-sided reconstruction.

These challenges are more pronounced in the regions of greatest scientific interest. Boundaries between the fluid and solid domains (the atmospheric surface layer, urban canopies, and ocean coastlines (Szanyi et al., 2016)) are precisely where the most significant exchanges of energy and moisture occur and where FTLE analysis is most consequential. Particle trajectories must be able to approach fluid-solid interfaces without artificially leaking into solid regions. This places the most stringent requirements on the interpolation scheme precisely where it is most difficult to apply.

We use the Parallelized Large-Eddy Simulation Model (PALM) (Maronga et al., 2015, 2020) as a case to illustrate these numerical challenges concretely. The simulations model a wildfire plume adjacent to a residential neighbourhood, where physically consistent FTLE boundaries will allow us to trace coherent structures in the flow and understand how fire, smoke and embers propagate downwind (Lin et al., 2025). PALM employs an Arakawa C-grid and a Cartesian domain. Buildings and topography are represented as solid masked regions, making it a representative example of the class of models for which these interpolation problems arise. The numerical issues demonstrated here, however, are not specific to PALM and will be encountered in any staggered-grid model with irregular solid boundaries.

This article presents a flux-conservative numerical solution to interpolating staggered velocity fields using mimetic vector interpolation (Pletzer and Fillmore, 2015; Pletzer and Hayek, 2019), which ensures that the velocity field satisfies the physically correct boundary conditions at fluid-solid interfaces. The result is a more physically consistent FTLE calculation that bridges the gap between the analytical theory of LCS and the realities of numerical model output, enabling reliable identification of coherent transport boundaries in complex geophysical flows.

https://doi.org/10.5194/egusphere-2026-3377
Preprint. Discussion started: 14 September 2026

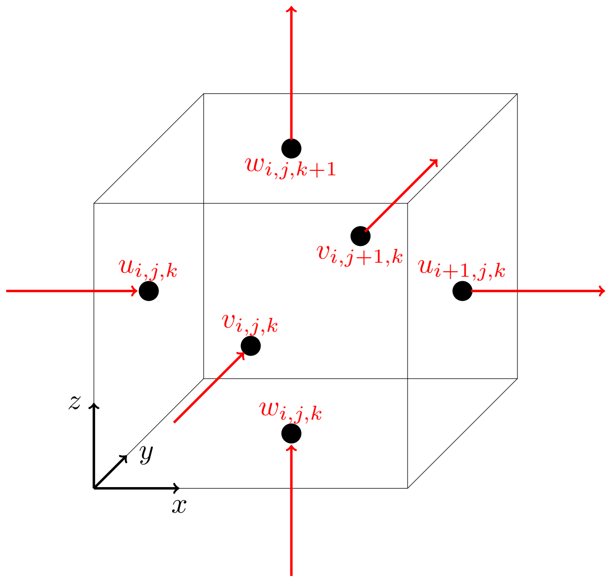

Figure 1. Staggering of the three-dimensional velocity field components according to the Arakawa C-grid.

2 How to compute FTLEs

Computing FTLEs involves the following steps: (1) trajectories are integrated along velocity field lines starting from a set of seed points; (2) the computation of the deformation matrix, which represents the rate at which neighbouring trajectories diverge or converge; and (3) the Lyapunov exponent is computed by estimating the largest eigenvalue of the symmetric Cauchy-Green tensor. For more details about FTLE, see Haller (2015) and Jarvis et al. (2024).

Integrating the trajectories requires one to be able to evaluate the velocity field at any point inside the domain. When the velocity is the result of a numerical simulation, velocities are only known at discrete locations, and interpolation is required.

Many computational fluid dynamics (CFD) codes rely on staggering the velocity field components (Arakawa and Lamb, 1977). Fig. 1 shows a cell of the grid with the u, v and w components of the velocity attached to different faces of the cell. Such staggerings are known to confer good numerical stability properties when solving the Navier-Stokes equation (Melvin et al., 2019).

Note that the velocity components u, v and w in Fig. 1 are not co-located. Most FTLE software (e.g. Jarvis and Ross (2025); Haller (2023)) assume these components to be co-located. Therefore, it is common to project all components to cell centres by averaging their values on opposite faces. This leads to issues at the boundaries of the domain, a half-cell-wide gap forms where data are missing for interpolation. One way to address this is by adding "ghost" cells, i.e. cells just outside the domain of interest, to be able to interpolate all the way to the boundary.

Fig. 2 illustrates how the use of ghost cells can introduce unphysical leakage across impermeable fluid-solid boundaries. In this example, the normal velocity at the boundary is prescribed to vanish. If a ghost cell with zero cell-centred velocity

https://doi.org/10.5194/egusphere-2026-3377
Preprint. Discussion started: 14 September 2026

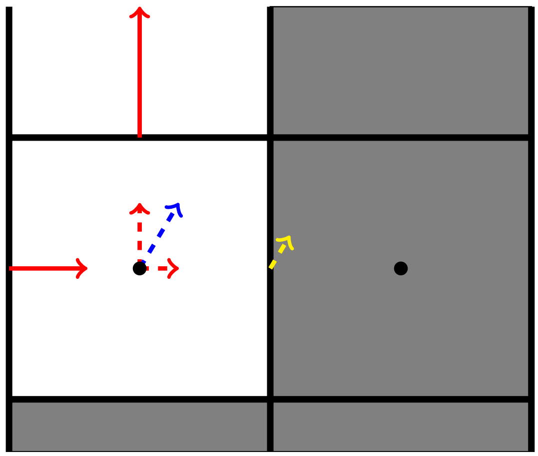

Figure 2. Example showing how an unphysical velocity can arise at the boundary when averaging components (e.g. u and v) to cell centres and adding a ghost cell. Shaded cells are outside the domain and have zero velocity. Red: Staggered u and v components on a C-grid. Blue: projection of the components to cell centre. Yellow: interpolated cell-centred velocity at the boundary has a component normal to the fluid-solid interface.

components is added inside the solid region to extend the interpolation stencil, interpolation between the fluid and ghost cell centres produces the yellow velocity vector shown in the figure. This interpolated velocity possesses a non-zero normal component at the interface, equal to one quarter of the normal velocity on the west side of the fluid cell. Because the resulting velocity is not tangential to the boundary, trajectory integration can produce numerical artefacts that effectively smear or erode the solid boundary. The appropriate remedy is to employ an interpolation scheme that remains valid throughout the fluid domain, including near boundaries, without requiring averaging to cell centres or the introduction of ghost cells. Naturally, such an interpolation scheme must allow for the tangential components to be discontinuous across the fluid-solid interface.

3 Mimetic vector interpolation

Physics aware (or fluid flow structure aware) interpolation techniques, referred to as “mimetic”, have been developed to address the limitations of standard scalar interpolation when applied to vector fields (Pletzer and Fillmore, 2015; Pletzer and Hayek, 2019; Pletzer et al., 2022). Unlike component-wise interpolation, mimetic methods are constructed to preserve fundamental conservation properties, such as fluxes across surfaces. They are therefore particularly well suited to staggered discretisations, including Arakawa C-grids. The key idea is to interpolate integral quantities, such as face-normal fluxes, rather than pointwise vector components. As a consequence, the reconstructed vector field satisfies discrete analogues of fundamental vector calculus identities, such as $\nabla \times \nabla(\cdot) = \mathbf{0}$ and $\nabla \cdot (\nabla \times \cdot) = 0$.

https://doi.org/10.5194/egusphere-2026-3377
Preprint. Discussion started: 14 September 2026

In the context of FTLE computations, mimetic interpolation offers several advantages: (i) it avoids the need to average velocity components to cell centres; (ii) it eliminates boundary gaps between cell centres and interfaces; (iii) it does not require ghost cells; and (iv) it allows particle trajectories to approach fluid-solid interfaces without artificial leakage into solid regions. In addition, mimetic methods naturally accommodate curvilinear coordinates, coordinate singularities, and invalid or masked cells.

Mimetic interpolation encompasses a family of methods, including linear, area-weighted, and volume-conservative schemes (Jones, 1999). Implementations are available in software frameworks such as Earth System Modeling Framework (ESMF) (ESMF, 2026) and Mimetic INTerpolation on the Sphere (MINT) (Pletzer and Hayek, 2019). An important and often overlooked aspect is that the choice of interpolation depends on the type of discrete field. For example, nodal (pointwise) fields are naturally interpolated using linear schemes, whereas cell-based quantities (e.g. densities) require volume-conservative interpolation, corresponding to piecewise-constant representations at lowest order. A volume-conservative interpolation conserves quantities, such as density, over a volume. This is important, for instance, in the case when a mass budget is invariant. Other mimetic interpolation methods conserve fluxes over surfaces, or line integrals over a path.

In the following, we outline the defining properties of mimetic interpolation for a three-dimensional pseudo-vector (bivector) field, extending the formulation of Pletzer et al. (2022) from Arakawa C-grids to fully three-dimensional settings. Bivectors arise when taking the cross product of two vectors, e.g. the velocity expressed from a stream function. We also highlight how these constructions ensure physically consistent behaviour at domain boundaries.

Let $\mathbf{u}$ denote a velocity field, and define its interpolation as

$$I_2\mathbf{u} = \sum_{i \in \text{faces}} \mu_i \, \mathbf{e}_i^{(2)}, \tag{1}$$

where the coefficients

$$\mu_i \equiv \int_{S_i} \mathbf{u} \cdot d\mathbf{S} \tag{2}$$

represent fluxes across cell faces S_i, and $\mathbf{e}_i^{(2)}$ are vector basis functions associated with each oriented face. Similarly, the interpolation of the divergence is defined as

$$I_3(\nabla \cdot \mathbf{u}) = \sum_{j \in \text{cells}} \nu_j \, e_j^{(3)}, \tag{3}$$

where ν_j are cell-based coefficients and $e_j^{(3)}$ are scalar basis functions. Note that I_2 and I_3 are not the same interpolation operator; the subscript emphasises the fact that each I conserves quantities on different dimensional manifolds (fluxes on surfaces for I_2 and densities within volumes for I_3).

A central requirement for mimetic interpolation is compatibility with the divergence theorem. For any control volume Ω, we require

$$\int_{\Omega} I_3(\nabla \cdot \mathbf{u}) \, dV = \int_{\Omega} \nabla \cdot (I_2\mathbf{u}) \, dV = \oint_{\partial\Omega} I_2\mathbf{u} \cdot d\mathbf{S}. \tag{4}$$

https://doi.org/10.5194/egusphere-2026-3377
Preprint. Discussion started: 14 September 2026

This condition is equivalent to the commutativity relation

$$I_3(\nabla\cdot\mathbf{u}) = \nabla\cdot(I_2\mathbf{u}), \tag{5}$$

i.e. interpolation and differentiation commute. Analogous constructions can be derived for the gradient and curl operators. An immediate consequence of Eq. (4) is that if $\mathbf{u}$ is divergence-free, then $\oint_{\partial\Omega} I_2\mathbf{u}\cdot d\mathbf{S} = 0$ so that flux conservation is preserved exactly.

$$\begin{tikzcd}
W_0 \arrow[r, "\nabla"] \arrow[d, "I_0"] & W_1 \arrow[r, "\nabla\times"] \arrow[d, "I_1"] & W_2 \arrow[r, "\nabla\cdot"] \arrow[d, "I_2"] & W_3 \arrow[d, "I_3"] \\
\widetilde{W}_0 \arrow[r, "\nabla"] & \widetilde{W}_1 \arrow[r, "\nabla\times"] & \widetilde{W}_2 \arrow[r, "\nabla\cdot"] & \widetilde{W}_3
\end{tikzcd}$$

Figure 3. A de Rham complex with mimetic interpolation operators I. W denote continuous function spaces and $\widetilde{W}$ their discretised counterpart. The application of a vector calculus operator and then the mimetic interpolation is equivalent to first interpolating then applying the operator. For example, mapping from W_2 to $\widetilde{W}_3$ can be achieved via W_3 or $\widetilde{W}_2$.

This structure is naturally interpreted in terms of a discrete de Rham complex (Fig. 3). The field $\mathbf{u}$ belongs to a function space W_2, while its interpolant lies in a subspace $\widetilde{W}_2 \subset W_2$. Likewise, $\nabla\cdot\mathbf{u} \in W_3$ and its interpolant lies in $\widetilde{W}_3 \subset W_3$. The commuting property ensures that applying a differential operator before or after interpolation yields the same result.

To enforce Eq. (4) at the level of individual cells, appropriate local basis functions must be constructed. For a hexahedral cell with parametric coordinates $0 \le \xi,\eta,\zeta \le 1$, low-order mimetic basis functions are given by Pletzer and Fillmore (2015)

$$\begin{aligned}\mathbf{e}_i^{(2)} \in \{&\xi\,\nabla\eta\times\nabla\zeta,\ -(1-\xi)\,\nabla\eta\times\nabla\zeta,\\ &\eta\,\nabla\zeta\times\nabla\xi,\ -(1-\eta)\,\nabla\zeta\times\nabla\xi,\\ &\zeta\,\nabla\xi\times\nabla\eta,\ -(1-\zeta)\,\nabla\xi\times\nabla\eta\}.\end{aligned} \tag{6}$$

These correspond to the six faces of the cell and are defined such that their flux contribution on each face is pointing outward (Fig. 4). At lowest order, the divergence space is spanned by a single basis function,

$$e^{(3)} = \nabla\xi\cdot(\nabla\eta\times\nabla\zeta). \tag{7}$$

To verify the commuting property, consider a single cell:

$$I_3(\nabla\cdot\mathbf{u}) = \nu\, e^{(3)} = \sum_i \mu_i\,\nabla\cdot\mathbf{e}_i^{(2)}. \tag{8}$$

Each divergence $\nabla\cdot\mathbf{e}_i^{(2)}$ evaluates to $e^{(3)}$. For example,

$$\nabla\cdot(\xi\nabla\eta\times\nabla\zeta) = \nabla\xi\cdot(\nabla\eta\times\nabla\zeta) + \xi\,\nabla\cdot(\nabla\eta\times\nabla\zeta) = \nabla\xi\cdot(\nabla\eta\times\nabla\zeta), \tag{9}$$

https://doi.org/10.5194/egusphere-2026-3377
Preprint. Discussion started: 14 September 2026

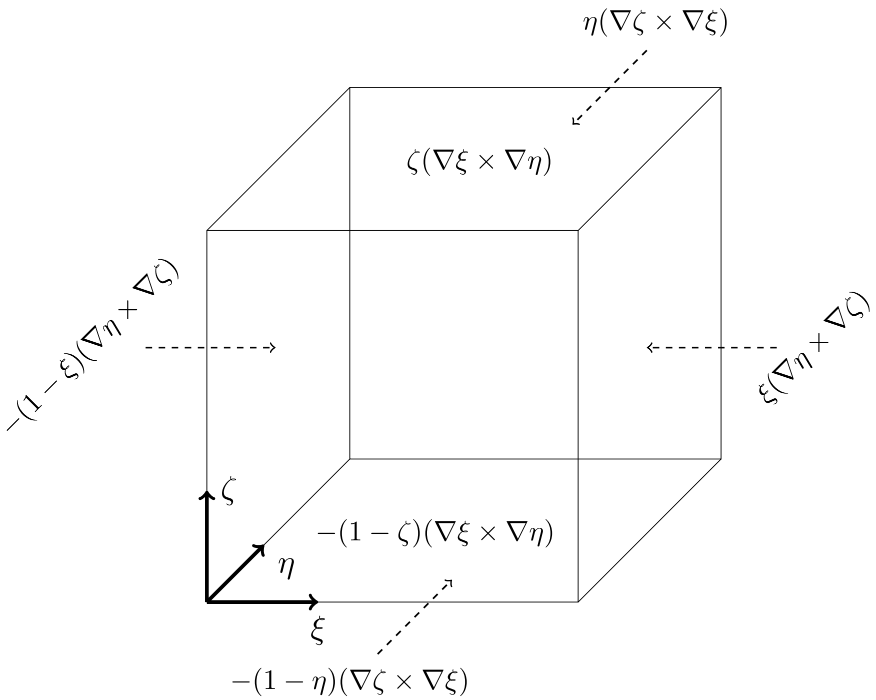

Figure 4. A schematic of a hexahedral cell with parametric coordinates $(\xi, \eta, \zeta) \in [0,1]^3$. The six vector basis functions $\mathbf{e}_i^{(2)}$ are shown on the faces where they have a non-zero flux contribution. The dashed arrows point to the four vertical faces.

since $\nabla \cdot (\nabla \times \cdot) = 0$ and $\nabla \times (\nabla \cdot) = 0$. Therefore, the equality Eq. (5) holds provided that

$$\nu = \int_{\text{cell}} \nabla \cdot \mathbf{u}\, dV = \sum_i \int_{S_i} \mathbf{u} \cdot d\mathbf{S} = \sum_i \mu_i, \tag{10}$$

which is precisely a discrete form of the divergence theorem. Thus, conservation is enforced locally on each cell.

Finally, consider a fluid cell adjacent to a solid boundary. Impermeability requires that the normal flux vanish on the boundary face, i.e. $\mu_i = 0$. However, tangential velocity components may remain finite within the fluid. The basis functions in Eq. (6) are constant in directions tangential to each face, allowing for discontinuities in tangential velocity across the interface. This naturally enforces slip boundary conditions and yields a physically consistent representation of the flow near solid obstacles.

4 FTLE Application to Fire Simulations

PALM has a rectilinear grid in x, y and z with a possibly varying cell size Δz. The interpolation basis functions from Eq. (6) then simplify to

$$\left\{ \frac{\xi}{\Delta y \Delta z}\hat{\mathbf{x}}, -\frac{1-\xi}{\Delta y \Delta z}\hat{\mathbf{x}}, \frac{\eta}{\Delta z \Delta x}\hat{\mathbf{y}}, -\frac{1-\eta}{\Delta z \Delta x}\hat{\mathbf{y}}, \frac{\zeta}{\Delta x \Delta y}\hat{\mathbf{z}}, -\frac{1-\zeta}{\Delta x \Delta y}\hat{\mathbf{z}} \right\} \tag{11}$$

https://doi.org/10.5194/egusphere-2026-3377
Preprint. Discussion started: 14 September 2026

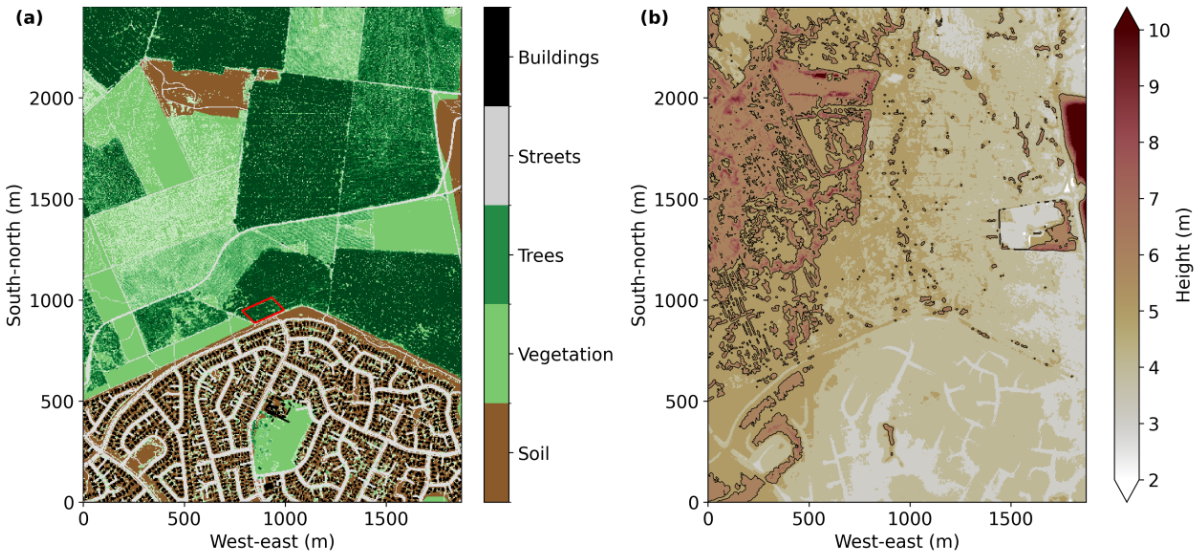

Figure 5. (a) Land use information of the PALM simulation domain with the red box marking the prescribed fire location. (b) Topographic map of the PALM domain (elevation above sea level) with terrain higher than 5 m highlighted by black contour lines.

where i,j,k are the cell indices, $\xi = (x - x_i)/\Delta x$, $\eta = (y - y_j)/\Delta y$, $\zeta = (z - z_k)/\Delta z$, x_i, y_j, z_k are the lower corner cell coordinates, and $\hat{\mathbf{x}}$, $\hat{\mathbf{y}}$, $\hat{\mathbf{z}}$ are the unit vectors in the x, y, z directions. The interpolation then becomes:

$$\begin{aligned} I_2\mathbf{u} = &(\xi u_{i+1,j,k} - (1-\xi) u_{i,j,k})\hat{\mathbf{x}} \\ &+ (\eta v_{i,j+1,k} - (1-\eta) v_{i,j,k})\hat{\mathbf{y}} \quad + (\zeta w_{i,j,k+1} - (1-\zeta) w_{i,j,k})\hat{\mathbf{z}} \end{aligned} \tag{12}$$

within each straight hexahedral cell (Fig. 1). This formula is then used to reconstruct the vector field at any point inside the cell.

To demonstrate the impact of mimetic interpolation in the numerical application of FTLEs, we use a large eddy simulation for a fire in Bottle Lake Forest, Christchurch, New Zealand (for more information see Lin et al. (2025)). This simulation, performed using the PALM model at a 4 m grid spacing, was designed to resolve turbulent-scale heat transport at a complex wildland-urban interface, where forests and residential areas are in close proximity. The prevailing wind is north-westerly, and the atmospheric boundary layer is near-neutral stability. As shown in Fig. 5, the domain features heterogeneous land-use and complex topography. The buildings are one- to two-storey residential houses, approximately 4-5 m in height. The atmosphere is inherently turbulent. Coupled with these surface complexities, heat transport becomes highly irregular, making it difficult to isolate flow structures using conventional diagnostic methods (Lin et al., 2025). This motivates the use of FTLE to identify the underlying coherent flow structures. In this context, the fire prescribed near the middle of the domain (Fig. 5a), located at the northern point of the residential area, serves as a critical test case where the physical consistency of the underlying interpolation scheme directly impacts the identification of these structures (also highlighted by the high FTLE values in Fig. 6a-d).

https://doi.org/10.5194/egusphere-2026-3377
Preprint. Discussion started: 14 September 2026

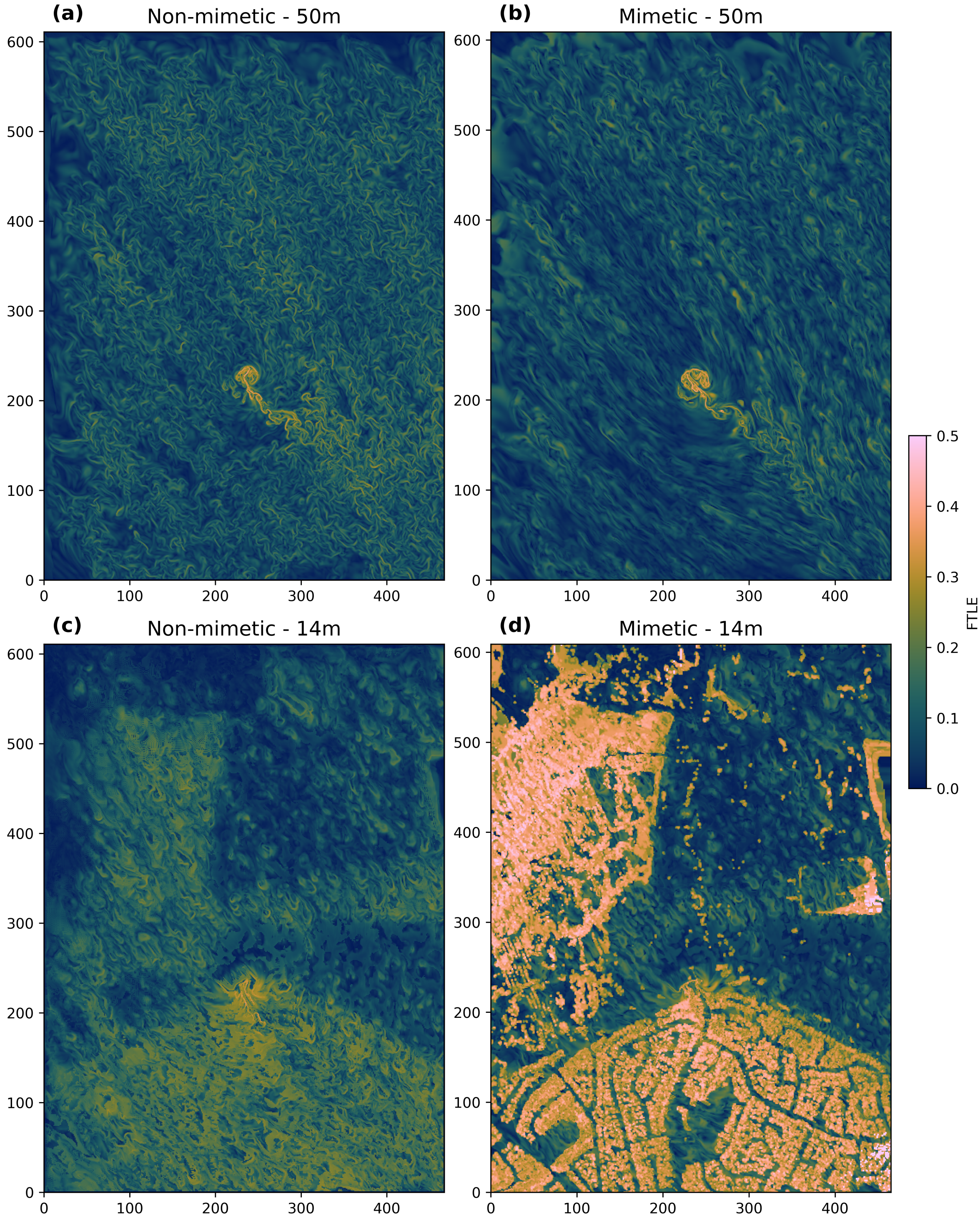

Figure 6. Comparison between non-mimetic cell averaging (a,c) and mimetic (b,d) FTLE at 50 m and 14 m above the surface from PALM simulations for a fire in a wildland-urban interface domain. FTLE fields in pink in (d) highlight where the interpolation issues were overlooked without the mimetic interpolation.

https://doi.org/10.5194/egusphere-2026-3377
Preprint. Discussion started: 14 September 2026

For the FTLE calculation, we used a 10 second backward integration from a start time 17 minutes after the fire begins. Integration time of 10 seconds was shown by Aksamit et al. (2024) to adequately resolve LCS in turbulent flows that become loosely defined at longer integration times.

Fig. 6 compares the FTLE results using non-mimetic and mimetic interpolation at 14 m, the lowest level available for both methods, and 50 m above the ground. At 14 m, the flow is strongly influenced by the land surface, buildings, and topography, but this influence weakens at 50 m. The non-mimetic calculation averages the velocity components to the cell centres to co-locate the components and then applies a cubic spline interpolation to smooth the data, whereas the mimetic interpolation maintains the staggered Arakawa C-grid. The greatest difference between the non-mimetic versus mimetic techniques (Fig. 6) can be seen nearest the surface at 14 m. The urban and topography footprint near the ground is only seen in the mimetic method. This is because PALM uses a Cartesian (non-terrain-following) grid, and masks grid points that lie below the terrain surface or within solid obstacles as NaNs. Furthermore, the FTLE filaments at 14 m for mimetic interpolation are crisp, though the structures are similar in shape. At 50 m above the surface, mimetic interpolation produces shear-driven u-shaped structures whereas in non-mimetic, the structures are smaller chaotic filaments. Notably, the positive heat flux divergence over a fire results in a warmer atmosphere, positive buoyancy, and increased near-surface inflow velocity, which is reflected in the mimetic FTLE field by longer filaments being drawn into the plume. Compared with the non-mimetic interpolation, mimetic interpolation yields an FTLE field that is more physically consistent with the underlying dynamics. Finally, mimetic interpolation allows the FTLE structures to be inferred to the bottom, top and lateral boundaries, reaching the lowest level of 10 m in this case (not shown). This near-boundary information is inaccessible with the non-mimetic interpolation.

5 Conclusions

This paper addresses a key gap in computing FTLEs from numerical model data by developing a physically consistent interpolation method for staggered-grid velocity fields. Like many other postprocessing tasks, it is common to require vector field components to be co-located. Simulations, however, often rely on staggered vector fields. An outcome of this work is to show that the co-location assumption can be removed from FTLE calculations, provided that care is taken to ensure conservation of fluxes, yielding more physically realistic vector fields near boundaries. In the case of the PALM code, the presence of buildings and other structures influences FTLE geometries. Specifically, we showed that mimetic based interpolation for FTLE is able to reveal the footprint of the urban topography. This is possible because mimetic interpolation preserves the channelling of the fluid by the solid obstacle (buildings, terrain, coastlines, etc.), rather than leaking into it artificially. The application of mimetic interpolation to FTLE (and to other LCS) analysis is critical for obtaining physically-correct coherent structure geometries from numerical simulations.

The mimetic interpolation applied in this work could find applications in other domains, for instance, computing the mass balance from flow across irregular surfaces. Note that a common impediment to saving staggered vector data was until recently the lack of a file format and schema. However, with the development of the UGRID conventions, which are part of the Climate

https://doi.org/10.5194/egusphere-2026-3377
Preprint. Discussion started: 14 September 2026

and Forecast (CF) conventions (Hassell et al., 2017), it is now possible to attach vector field data to cell edges or faces. Our recommendation therefore, is to save simulation output data in ways that faithfully respect the discretisation of the model.

Code and data availability. The code and data used in this study are openly available in https://github.com/pletzer/pv_ftle and at https://doi.org/10.5281/zenodo.20060141 (Pletzer, 2026). Static data for PALM (blf_night_loc1_4m_static) is available at https://doi.org/10.5281/zenodo.14532905 (Lin, 2024).

Author contributions. TP, AP and MK: conceptualisation. AP: derived the mimetic interpolation method and wrote Sections 2 and 3. AP and TCA: designed Figs 1, 2 and 4. TCA: designed Fig 3 and reviewed derivations. TP: wrote Sections 1, 4 and 5 and produced Fig 6. DL: conducted the PALM simulations and produced Fig 5. All authors contributed to edits.

Competing interests. The authors report no conflict of interest.

Acknowledgements. The authors acknowledge a research consultancy with Research and Education Advanced Network New Zealand (REANNZ) Ltd. funded by the Ministry of Business, Innovation & Employment. Generative AI tools (ChatGPT and Claude) have been used for grammar and language polishing during manuscript preparation. Following the use of this tool, all content has been edited and reviewed. We take full responsibility for the content of this publication.

Financial support. This research was funded by the Royal Society of New Zealand (grant no. RDF-UOC1701). DL acknowledges support from the Australian Research Council (ARC) Centre of Excellence for Climate Extremes (Project CE170100023).

https://doi.org/10.5194/egusphere-2026-3377
Preprint. Discussion started: 14 September 2026

References

Aksamit, N., Katurji, M., and Zhang, J.: Understanding Coherent Turbulence and the Roll-Cell Transition With Lagrangian Coherent Structures and Frame-Indifferent Fluxes, Journal of Geophysical Research: Atmospheres, 129, https://doi.org/10.1029/2024JD041490, 2024.

Arakawa, A. and Lamb, V.: Computational design of the basic dynamical processes of the UCLA general circulation model, Methods in Computational Physics, 17, 174–265, 1977.

ESMF: Earth System Modeling Framework, http://www.earthsystemmodeling.org/, 2026.

Haller, G.: Lagrangian coherent structures, Annual Review of Fluid Mechanics, 47, 137–162, https://doi.org/10.1146/annurev-fluid-010313-141322, 2015.

Haller, G.: Transport Barriers and Coherent Structures in Flow Data, in: Transport Barriers and Coherent Structures in Flow Data, chap. 5, pp. 141–176, Cambridge University Press, https://doi.org/10.1017/9781009225199.012, 2023.

Hassell, D., Gregory, J., Blower, J., Lawrence, B. N., and Taylor, K. E.: A data model of the Climate and Forecast metadata conventions (CF-1.6) with a software implementation (cf-python v2.1), Geoscientific Model Development, 10, 4619–4646, https://doi.org/10.5194/gmd-10-4619-2017, 2017.

Jarvis, A. and Ross, S. D.: NumbaCS: A fast Python package for coherent structure analysis, Journal of Open Source Software, 10, 7948, https://doi.org/10.21105/joss.07948, 2025.

Jarvis, A., Hossein Mardi, A., Foroutan, H., and Ross, S. D.: Atmospheric transport structures shaping the “Godzilla” dust plume, Atmospheric Environment, 333, 120 638, https://doi.org/10.1016/j.atmosenv.2024.120638, 2024.

Jones, P. W.: First- and Second-Order Conservative Remapping Schemes for Grids in Spherical Coordinates, Monthly Weather Review, 127, 2204–2210, https://doi.org/10.1175/1520-0493(1999)127<2204:FASOCR>2.0.CO;2, 1999.

Lin, D.: PALM input files for WUI [data set], https://doi.org/10.5281/zenodo.14532906, 2024.

Lin, D., Katurji, M., Zawar-Reza, P., Malyarenko, A., Valencia, A., and Zhang, J.: High-Fidelity Experimental Simulations of Atmospheric Flow Near Low-Intensity Fires in a Wildland-Urban Interface, Journal of Geophysical Research: Atmospheres, 130, https://doi.org/10.1029/2025JD043641, 2025.

Maronga, B., Gryschka, M., Heinze, R., Hoffmann, F., Kanani-Sühring, F., Keck, M., Ketelsen, K., Letzel, M. O., Sühring, M., and Raasch, S.: The Parallelized Large-Eddy Simulation Model (PALM) version 4.0 for atmospheric and oceanic flows: model formulation, recent developments, and future perspectives, Geoscientific Model Development, 8, 2515–2551, https://doi.org/10.5194/gmd-8-2515-2015, 2015.

Maronga, B. et al.: Overview of the PALM model system 6.0, Geoscientific Model Development, 13, 1335–1372, https://doi.org/10.5194/gmd-13-1335-2020, 2020.

Melvin, T., Benacchio, T., Shipway, B., Wood, N., Thuburn, J., and Cotter, C.: A mixed finite-element, finite-volume, semi-implicit discretisation for atmospheric dynamics: Cartesian geometry, Quarterly Journal of the Royal Meteorological Society, 145, 2835–2853, https://doi.org/10.1002/qj.3501, 2019.

Pletzer, A.: pletzer/pv_ftle: pv_ftle 0.9.2 [code], https://doi.org/10.5281/zenodo.20060141, 2026.

Pletzer, A. and Fillmore, D.: Conservative Interpolation of Edge and Face Data on N Dimensional Structured Grids Using Differential Forms, Journal of Computational Physics, 302, 21–40, https://doi.org/10.1016/j.jcp.2015.08.029, 2015.

Pletzer, A. and Hayek, W.: Mimetic Interpolation of Vector Fields on Arakawa C/D Grids, Monthly Weather Review, 147, 3–16, https://doi.org/10.1175/MWR-D-18-0146.1, 2019.

https://doi.org/10.5194/egusphere-2026-3377
Preprint. Discussion started: 14 September 2026

Pletzer, A., Behrens, E., and Little, B.: MINT: A Library That Conserves Vorticity or Lateral Fluxes When Interpolating Vector Fields, in: Proceedings of the Platform for Advanced Scientific Computing Conference, PASC '22, Association for Computing Machinery, New York, NY, USA, https://doi.org/10.1145/3539781.3539786, 2022.

Spaulding, M. L.: State of the art review and future directions in oil spill modeling, Marine Pollution Bulletin, 115, 7–19, https://doi.org/10.1016/j.marpolbul.2017.01.001, 2017.

Szanyi, S., Lukovich, J. V., and Barber, D. G.: Lagrangian analysis of sea-ice dynamics in the Arctic Ocean, Polar Research, 35, 30 778, https://doi.org/10.3402/polar.v35.30778, 2016.

Veatch, J. M., Oliver, M. J., Fredj, E., Statscewich, H., Bernard, K., Hann, A. M., Voirol, G., Fuchs, H. L., Fraser, W. R., and Kohut, J. T.: Lagrangian coherent structures influence the spatial structure of marine food webs, Communications Earth & Environment, 6, 127, https://doi.org/10.1038/s43247-025-02101-x, 2025.